Original Article

MOLECULAR METABOLISM

NPY derived from AGRP neurons controls feeding via Y1 and energy expenditure and food foraging behaviour via Y2 signalling

Yue Qi [1,2,4], Nicola J. Lee [1,2,4], Chi Kin Ip [1,2,4], Ronaldo Enriquez [1], Ramon Tasan [3], Lei Zhang [1,2], Herbert Herzog [1,2,*]

ABSTRACT

Objective: Aguti-related protein (AGRP) neurons in the arcuate nucleus of the hypothalamus (ARC), which co-express neuropeptide Y (NPY), are key regulators of feeding and energy homeostasis. However, the precise role NPY has within these neurons and the specific pathways that it control are still unclear. In this article, we aimed to determine what aspects of feeding behaviour and energy homeostasis are controlled by NPY originating from AGRP neurons and which Y-receptor pathways are utilised to fulfil this function.

Methods: Novel conditional $Agrp^{cre/+};Npy^{lox/lox}$ knockout mice were generated and comprehensively phenotyped, both under standard chow as well as high-fat-diet conditions. Designer receptor exclusively activated by designer drugs (DREADD) technology was used to assess the altered responses on feeding and energy homeostasis control in the absence of NPY in these neurons. Rescue experiments utilising Npy1r- and Npy2r-selective NPY ligands were performed to assess which component of the energy homeostasis control is dependent by which specific Y-receptor pathway.

Results: We show that the specific deletion of *Npy* only in AGRP neurons leads to a paradoxical mild obese phenotype associated with reduced locomotion and energy expenditure and increased feeding and Respiratory Quotient (RQ) that remain elevated under a positive energy balance. The activation of *Npy*-deficient AGRP neurons via DREADD's is still able to drive feeding, yet with a delayed onset. Additionally, Clozapine-N-oxide (CNO) treatment reduces locomotion without impacting on energy expenditure. Rescue experiments re-introducing Npy1r- and Npy2r-selective NPY ligands revealed that the increased feeding and RQ are mostly driven by Npy1r, whereas energy expenditure and locomotion are controlled by Npy2r signalling.

Conclusion: Together, these results demonstrate that NPY originating from AGRP neurons is not only critical to initiate but also for continuously driving feeding, and we for the first time identify which Y-receptor controls which pathway.

Keywords NPY; Food intake; Obesity; Knockout mice; AGRP; Npy1r

1. INTRODUCTION

A complex neuronal regulatory network has developed in the brain, specifically in the hypothalamus to coordinate feeding and energy homeostasis regulation [1]. This system has the capacity to sense the amount of energy stored in the body and adjusts food intake and fuel consumption, so that body temperature and body weight stay reasonably constant, despite variations in daily food intake and energy expenditure [2,3]. Especially under conditions of a negative energy balance, a variety of actions are initiated through hypothalamic circuits that turn on energy-conserving pathways, thereby reducing energy expenditure. Equally important is that food foraging and food intake are also strongly stimulated. The first and foremost regulators of these processes are NPY/Aguti-related protein (AGRP) neurons within the hypothalamus. Specifically, *Npy* in the arcuate nucleus of the hypothalamus (ARC) is strongly upregulated by a negative energy balance, and when chronically administered with free access to food, this leads to a strong increase in food intake and the development of obesity. However, the NPY function has also been linked to other aspects of food intake [4], the control of glucose [5], bone homeostasis [6], several feeding-related behaviours [7], food-odour attraction [8], as well as physical activity [9]. Thus, the NPY system may have an integrating role in coordinating feeding, locomotor activity, and energy homeostasis particularly under stressful conditions such as diminished food availability.

Because *Npy* is also expressed at high levels throughout the brain, most investigations into NPY's role in feeding and energy homeostasis control have been conducted with tools that rely on the transcription of *Agrp*, with whom *Npy* is co-localised and whose expression is restricted to the ARC. Although many important insights have been gained by this approach, the specific contribution of NPY to the

[1]Neuroscience Division, Garvan Institute of Medical Research, St Vincent's Hospital, Darlinghurst, NSW 2010, Australia [2]St Vincent's Clinical School, UNSW Sydney, Sydney, NSW, Australia [3]Department of Pharmacology, University of Innsbruck, Innsbruck, Austria

[4] These authors contributed equally to this article.

*Corresponding author. Neuroscience Division, Garvan Institute of Medical Research, St Vincent's Hospital, Darlinghurst, NSW 2010, Australia. E-mail: h.herzog@garvan.org.au (H. Herzog).

Received November 1, 2021 • Revision received January 31, 2022 • Accepted February 3, 2022 • Available online 12 February 2022

https://doi.org/10.1016/j.molmet.2022.101455

different physiological processes that are controlled by this neuronal population is still unclear. Global germline knockout models for both *Agrp* and *Npy* have been generated, but surprisingly, they show very little effect on altering food intake or energy homeostasis under baseline conditions [10]. Similarly, double knockout models of *Agrp* and *Npy* do not reveal any dramatic effect on feeding-related behaviours, suggesting that strong compensatory mechanisms are in place to overcome the loss of *Npy* and *Agrp* signalling [11]. An neonatal ablation of the entire AGRP neuronal population is also tolerated. Importantly, however, an adult-onset ablation of these neurons leads to lethality in a short period because of the complete termination of feeding and resulting starvation [12,13]. Recently, models utilising *Agrp*-Cre driver lines on the background of the global *Npy* knockout have been generated and analysed [4,14]; however, because of the global deletion of *Npy*, the results are obscured and do not address the specific function of NPY in AGRP neurons. Therefore, we have generated a conditional *Npy* knockout model that restricts the deletion of *Npy* to only AGRP neurons and utilised a comprehensive phenotyping paradigm combined with Designer receptor exclusively activated by designer drugs (DREADD) technology and rescue studies to decipher the specific role NPY has in AGRP neurons on the control of feeding behaviour and energy homeostasis. These studies revealed that NPY originating from AGRP neurons controls feeding initiation predominantly via Npy1r signalling and locomotor activity and energy expenditure via Npy2r signalling. NPY in AGRP neurons also seems to be critical for maintaining glucose homeostasis and matching bone mass to body weight.

2. MATERIALS AND METHODS

2.1. Animals

Mice lacking *Npy* in AGRP neurons ($Agrp^{cre/+};Npy^{lox/lox}$ mice) were generated by crossing *Npy* floxed ($Npy^{lox/lox}$) mice [15] with mice expressing Cre under the control of the *Agrp* promotor ($Agrp^{cre/+}$ mice) [16]. Heterozygous $Agrp^{cre/+};Npy^{lox/+}$ mice were used as controls. All animal experiments were approved by the Garvan Institute/St Vincent's Hospital Animal Experimentation Ethics Committee and conducted in accordance with relevant guidelines and regulations. Mice were housed under conditions of controlled temperature (22 °C ± 1 °C) with a 12-h light, 12-h dark cycle (lights on at 0700). Mice had *ad libitum* access to either a standard chow diet (8% calories from fat, 21% calories from protein, 71% calories from carbohydrate, and 3.1 kcal/g; Gordon's Speciality Stock Feeds, Yanderra, NSW, Australia) or a high-fat diet (HFD; 43% calories from fat, 17% calories from protein, 40% calories from carbohydrate, and 4.78 kcal/g; Specialty Feeds, Glen Forrest, WA, Australia) from 6 weeks of age. Body weight was monitored weekly.

2.2. Metabolic phenotyping of mice

Indirect calorimetry measurements on mice were performed using the Promethion metabolic cage system (Sable Systems International, Las Vegas, NV, USA). Mice were acclimatised for 72 h in the Promethion system before data acquisition began. The Promethion multiplexed system has a 'home-like' environment with each cage containing standard bedding, a food hopper, a water bottle, and an enrichment tube for body mass measurements, all connected to load cells for real-time weight monitoring. Food spillage was collected at the end of the run from each cage, and food intake was corrected accordingly. Instrument control and data acquisition were performed according to the manufacturer's instructions. Raw data were processed using ExpeData software (Sable Systems).

Whole body lean mass, fat mass, bone mineral content (BMC), and bone mineral density (BMD) were measured in mice anesthetised with isoflurane using a dedicated mouse dual X-ray absorptiometry (DXA) (Lunar Piximus II, GE Medical Systems, Madison WI) at 14 weeks of age.

2.3. Open-field test

Adult mice were acclimatized in the experimental room for at least 48 h under controlled temperature (22 °C ± 1 °C) with a 12-h light, 12-h dark cycle (lights on at 0700) at an illumination of 200 Lux during the light phase. The open-field (OF) chamber measured a dimension of 50 cm × 50 cm x 50 cm with the inner zone defined as 37.5 cm square. To test the level of anxiety-like behaviour, mice were placed into the centre of the chamber, and the activity of the mice was tracked by using the video tracking stimulator system (Teleopto). This software provides data on the location of the mice at a 0.5-s interval with x- and y-axis coordinates recorded. A scatter plot was generated for each mouse to visualize its activity over a 10-min timeframe. The percentage of time spent in the inner zone and the outer zone was calculated, as well the total distance travelled (m).

2.4. Tissue collection

Mice were culled between 13.00 and 16.00 h by cervical dislocation and decapitation. Brains were collected and frozen flat on dry ice and then stored at −80 °C. The interscapular brown adipose tissue (BAT) and white adipose tissue (WAT) from the inguinal, epididymal, retroperitoneal, and mesenteric deposits were excised and weighed. The organs, including the gonads, spleen, pancreas, kidney, liver, and heart, were also excised and weighed.

For the collection of tissue required for immunohistochemistry, whole animal perfusion fixation was performed. Briefly, after complete anaesthesia, the mouse was perfused with 0.9% saline through the left ventricle, followed by 4% paraformaldehyde perfusion until the whole body was fully fixed. The brain was removed from the skull, placed in fixative for 2 h at 4 °C, and kept in 30% glucose in PBS over 24 h or until brain sunk and then stored at −80 °C until further use.

2.5. Brain injection for Adeno associated virus (AAV)-DREADD and AAV-NPY intervention

To deliver DREADD's as well as NPY ligands specifically into *Agrp* neurons, FLEX technology was used. Mice were fully anesthetized with a saline-diluted ketamine/xylazine cocktail according to their body weight and placed on the stereotaxic frame. Surgical incisions were made through full anatomic layers of the skin, periosteum, and skull to expose the surface of the brain. A microinjection needle was adjusted over the brain towards the ARC according to the coordinates from the Maps of Mouse Brain [17]. A hole was then drilled through the dura and sagittal sinus followed by the insertion of the injection needle. The depth of the injection was also adjusted to specifically target the ARC; 0.5−1 μl of the injection solution containing AAV (4×10^{12}) was then slowly injected over 5 min, and the needle was left in place for another 10 min to prevent reflux. The same procedure was performed on the collateral side. After the injection and removal of the needle, the wound was sutured, and the animal was housed individually in a cage with a heating pack until it fully woke up. Medical indications including body weight, physical movement, and infection were regularly monitored for two weeks after the injection until the mice were fully recovered.

2.6. RNAscope™ *in situ* hybridization

RNAscope™ technology, a non-radioactive *in situ* hybridization assay, was used specifically to detect co-localisation in mRNA expression. In

brief, fresh-frozen brains were cryosectioned at 25 μm thickness, placed onto SuperFrost Plus slides, and stored at −20 °C until use. Sections through the ARC were used for RNAscope™ *in situ* hybridisation following the manufacturer's protocol, using specifically designed RNAscope™ probes complementary to the mRNA of *Npy* (Cat No: 313,321), *Agrp* (Cat No: 400,711), *Pomc* (Cat No: 314,081), *Npy1r* (Cat No: 427,021), *Npy2r* (Cat No: 315,951), *Vglu2* (Cat No: 319,171-C3), and *Vgat* (Cat No: 319,191-C3), and the section slides were stored in 5 x SSC at room temperature overnight.

Two types of RNAscope™ detection reagent kits were used: chromogenic (Cat No: 322,500) and fluorescent (Cat No: 320,851). Light, fluorescent, and confocal microscopes (Carl Zeiss, Germany) were used to examine the results, and high-resolution photos were taken with an attached microscopic camera.

2.7. Bone micro-computed tomography (μCT)

The μCT analysis of femora was performed as previously described [18]. Briefly, after fixation, left femora were cleaned of the muscle, and analyses of the bone were performed by μ-CT with a Skyscan 1172 scanner and associated analysis software (Skyscan, Aartselaar, Belgium) as previously described [16]. Analyses of the cortical bone were performed in a region 1.0 mm in height, selected 2.5 mm proximally from the distal growth plate, resulting in calculations of the following parameters: total tissue area, bone area, marrow area, periosteal perimeter, cortical thickness, and polar moment of inertia (an index of strength). Analyses of the trabecular bone were performed in a region 1.0 mm in height, selected 0.5 mm proximally from the distal growth plate, resulting in calculations of the following parameters: total tissue volume, bone volume, trabecular number, trabecular thickness, and trabecular separation.

2.8. Immunohistochemistry

Fixed brains were cryosectioned at 40 μm thickness and stored in a cryoprotectant at 4 °C before immunohistochemical staining for cFOS. To compare the cFOS activity between brains, 5 brains per group were processed for immunohistochemistry, and one of every four rostral to caudal sections were selected for each brain for the analysis. After incubation in 6% H_2O_2 for 20 min to remove endogenous peroxides, the sections were then incubated in 10% normal goat serum for 1 h to block the non-specific binding sites, followed by incubation in 0.1 M phosphate-buffered saline containing 5% goat serum, 0.2% triton X100, 0.1% bovine serum albumin, and affinity-purified rabbit IgG polyclonal antibody against cFOS (1:1000) overnight. The following day, the sections were incubated with a biotinylated secondary antibody anti-rabbit (1:500) for 2 h and ExtraAvidin peroxidase (1:500) for another 2 h. DAB (3,3′-diaminobenzidine) substrate buffer with DAB chromogen (Dako North America, Inc.) was used to develop the staining, and the whole reaction was monitored using a light microscope. The cFOS-stained sections were then mounted on slides and coverslipped with Permamount. The number of the cFOS-stained neurons was counted by brightfield microscopy.

For fluorescent immunodetection, the H_2O_2 incubation step was omitted, and brain sections were incubated in 0.5% sodium borohydride (Aldrich, Lot#SHBC2411V) for 20 min to expose antigens. Slides were washed four times in 1 x PBS for 5 min each. Brain sections were incubated in a 10% normal goat serum for 1 h for blocking and then in the solution with a primary antibody at room temperature overnight. The primary antibody solution was prepared with the same buffers that were used in DAB reaction. After washing four times in 1 x PBS for 5 min each on the second day, brain sections were incubated at room temperature for 2 h in a corresponding fluorescent secondary antibody, according to the species in which the primary antibody was raised (Alexa 488 or 594, 1:500), followed by four washes in 1 x PBS for 5 min each. Sections were mounted on slides and coverslipped with anti-fade mount medium. Images were taken using a fluorescent microscope with camera (Leica).

2.9. Statistical analyses

All data are expressed as means ± SEM. Differences between groups were assessed using Student's *t* test, Analysis of variance (ANOVA) followed by the Bonferroni's multiple comparison post hoc test, or repeated-measures ANOVA where appropriate. Statistical analyses were performed with Prism, version 7 (GraphPad Software Inc, La Jolla, CA, USA). $P < 0.05$ was taken to be statistically significant.

3. RESULTS

3.1. Mice lacking *Npy* selectively only in AGRP neurons develop mild obesity

To investigate the function of NPY specifically in *Agrp*-positive neurons, we crossed our conditional *Npy* knockout line ($Npy^{lox/lox}$) [15] with an *Agrp*-Cre transgenic line ($Agrp^{cre/+}$) [16] to eventually produce $Agrp^{cre/+};Npy^{lox/lox}$ mice. Successful gene deletion was confirmed by the Polymerase chain reaction (PCR) analysis of genomic DNA isolated from the hypothalamus of these mice (Supplementary Figs. 1A—B). To evaluate the impact of the lack of *Npy* from AGRP neurons on energy homoeostasis under chow conditions, we performed the comprehensive metabolic profiling of $Agrp^{cre/+};Npy^{lox/lox}$ mice utilising the Promethion system. $Agrp^{cre/+};Npy^{lox/+}$ was chosen as the most appropriate and rigorous control because this is the only way to account for the potential contribution of the Cre-transgene as well as the floxed allele at the same time in the same littermates. Interestingly, and contrary to what would be expected from a lack of *Npy* in these neurons, $Agrp^{cre/+};Npy^{lox/lox}$ mice actually displayed a significant increase in food intake, specifically during the dark period, which was associated with an increase in bout size but not bout number (Figure 1A—D). Furthermore, during both the light and dark phases, they had significantly reduced activity levels (Figure 1E—F), significantly decreased energy expenditure both when normalised to body weight (data not shown) as well as to lean mass (Figure 1G—H), and significantly increased Respiratory Quotient (RQ) levels (Figure 1I—J). Interestingly, the elevation in RQ reached levels above 1.0 during the dark phase, suggestive of an induction of lipid synthesis. To determine whether their reduced activity levels may be influenced by an alteration in anxiety behaviour, we also tested these mice in an open-field test. However, there was no difference in the time spent in the inner versus the outer zone or in the distance travelled in the two zones (Supplementary Figs. 2A—D), excluding altered anxiety levels as a cause for the overall reduced physical activity.

Consistent with their increased food intake and lower activity levels, male $Agrp^{cre/+};Npy^{lox/lox}$ mice on a chow diet displayed a slightly higher body weight than control mice (Figure 1K) mainly because of an increase in fat mass with no change in lean mass (Figure 1L—M). The increase in fat mass was most prominent in the epididymal and mesenteric white adipose tissue depots (Figure 1N), whereas other tissues, with the exception of the liver, were not significantly increased in weight (Figure 1O). Interestingly, in response to a 24-hr fast, $Agrp^{cre/+};Npy^{lox/lox}$ mice lost significantly less body weight than control mice but also regained it at a slower rate and still had a significantly lower percentage body weight compared with control mice 24 h after re-feeding (Figure 1P). There were no differences in the associated food intake in the first 7 h of re-feeding; however, cumulative food intake was

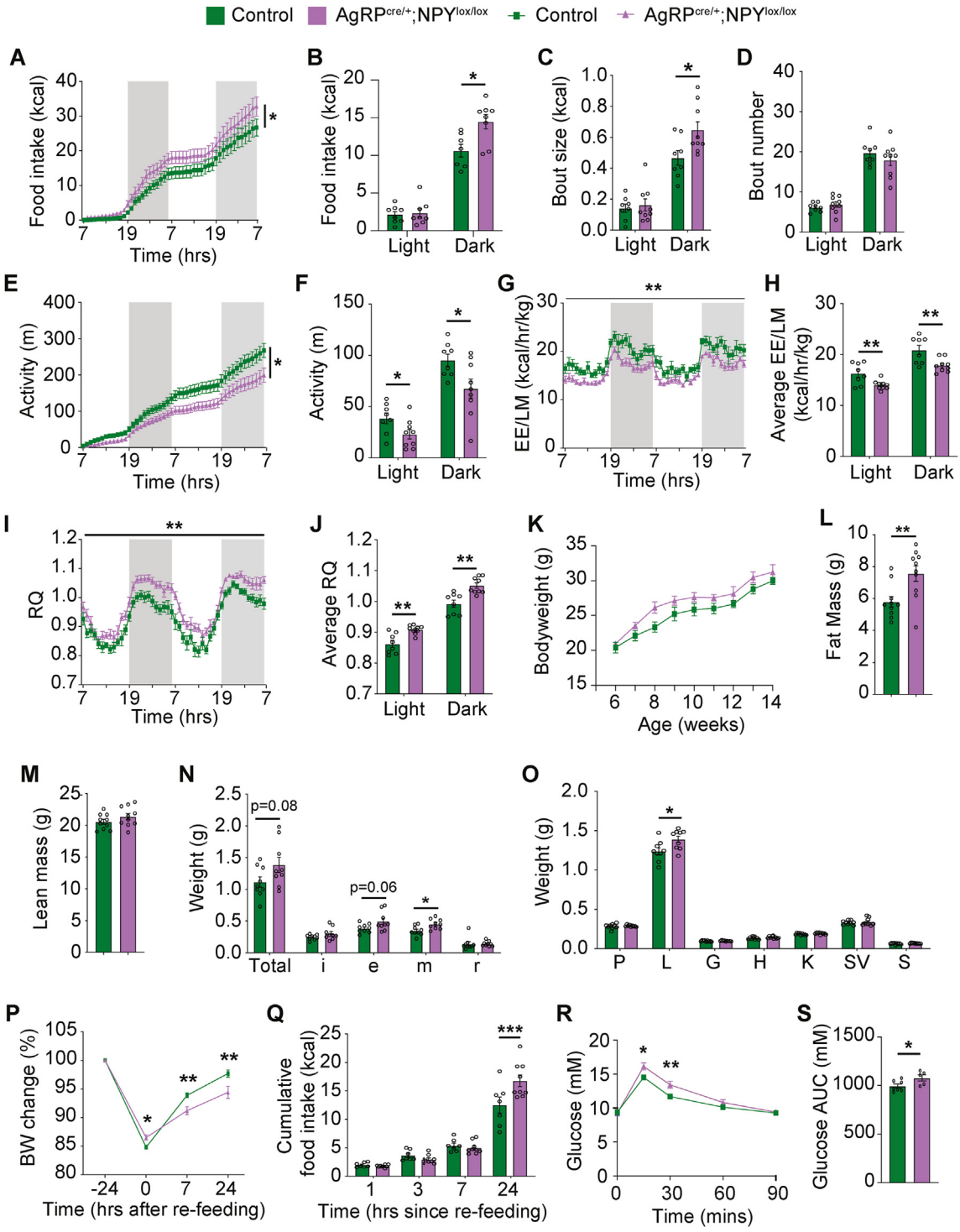

Figure 1: Mice lacking *Npy* selectively only in AGRP neurons develop mild obesity. (A) Cumulative food intake over a 48-hour time course and averaged 12-hour (B) food intake, (C) bout size, and (D) bout number during the light and dark phases in male *Agrp*$^{cre/+}$;*NPY*$^{lox/lox}$ and control mice. (E) Cumulative distance in voluntary locomotion travelled (activity) over a 48-hour time course and (F) averaged activity during the light and dark phases, (G) energy expenditure normalised to lean mass (EE/LM) over a 48-hour time course and (H) averaged EE/LM during the light and dark phases, and (I) respiratory quotient (RQ) over a 48-hour time course and (J) averaged RQ during the light and dark phases in male *Agrp*$^{cre/+}$;*NPY*$^{lox/lox}$ and control mice. (K) The body weight curve for male *Agrp*$^{cre/+}$;*NPY*$^{lox/lox}$ and *Agrp*$^{cre/+}$;*NPY*$^{lox/+}$ control mice on a chow diet. (L) Fat and (M) lean mass as measured by DXA and (N) summed and individual weights of white adipose tissue (WAT) from the inguinal (i), epididymal (e), mesenteric (m), and retroperitoneal (r) deposits at cull. (O) Weights of the pancreas (p), liver (l), gonads (g), heart (h), kidney (k), seminal vesicles (sv), and spleen (s) at cull. (P) Change in body weight during a 24-hour fast followed by 24 h of re-feeding and (Q) cumulative food intake during the 24 h of re-feeding in male *Agrp*$^{cre/+}$;*NPY*$^{lox/lox}$ and control mice. (R) Glucose levels and (S) glucose area under the curve (AUC) during a glucose tolerance test in male *Agrp*$^{cre/+}$;*NPY*$^{lox/lox}$ and control mice. Data are means ± SEM of at least 5 per group. * = $p < 0.05$, ** = $p < 0.01$, *** = $p < 0.001$ as indicated.

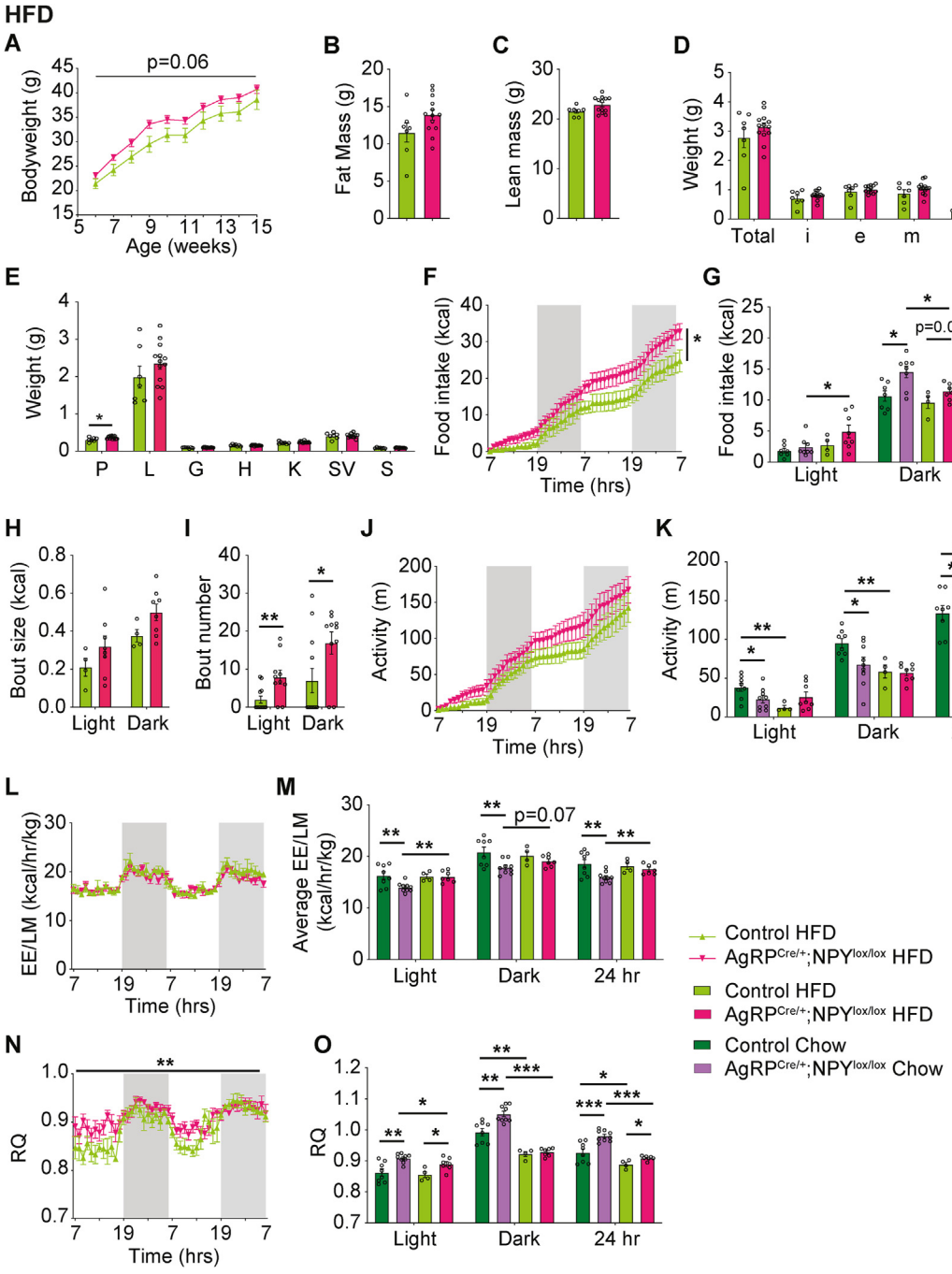

Figure 2: Lack of *Npy* in AGRP neurons alters energy homeostasis regulation under a positive energy balance. **(**A) The body weight curve for male *Agrp*$^{cre/+}$;*NPY*$^{lox/lox}$ and *Agrp*$^{cre/+}$;*NPY*$^{lox/+}$ control mice on an HFD. (B) Fat and (C) lean mass as measured by DXA and (D) summed and individual weights of white adipose tissue (WAT) from the inguinal (i), epididymal (e), mesenteric (m), and retroperitoneal (r) deposits at cull for male *Agrp*$^{cre/+}$;*NPY*$^{lox/lox}$ and control mice on an HFD. (E) Weights of the pancreas (p), liver (l), gonads (g), heart (h), kidney (k), seminal vesicles (sv), and spleen (s) at cull. (F) Cumulative food intake over a 48-hour time course, (G) averaged 12 h during the light and dark phases and total 24-hour food intake for male *Agrp*$^{cre/+}$;*NPY*$^{lox/lox}$ and control mice on a chow diet or an HFD. (H) Average bout size and (I) bout number during the light and dark phases for male *Agrp*$^{cre/+}$;*NPY*$^{lox/lox}$ and control mice on an HFD. (J) Cumulative distance in voluntary locomotion travelled (activity) over a 48-hour time course and (K) averaged activity during the light and dark phases as well as over 24 h, (L) energy expenditure normalised to lean mass (EE/LM) over a 48-hour time course and (M) averaged EE/LM during the light and dark phases as well as over 24 h, (N) respiratory quotient (RQ) over a 48-hour time course and (O) averaged RQ during the light and dark phases as well as over 24 h in male *Agrp*$^{cre/+}$;*NPY*$^{lox/lox}$ and control mice on a chow diet or an HFD. Data are means ± SEM of at least 4 per group. * = $p < 0.05$, ** = $p < 0.01$, *** = $p < 0.001$ as indicated.

significantly higher at the 24-hour timepoint in *Agrp*$^{cre/+}$;*Npy*$^{lox/lox}$ mice (Figure 1Q). Consistent with their mild obesity, male *Agrp*$^{cre/+}$;*Npy*$^{lox/lox}$ mice displayed impaired glucose tolerance compared with control mice with significantly higher glucose levels at the 15- and 30-minute timepoints (Figure 1R–S). Interestingly, despite their increased fat mass, basal glucose levels were unaltered from controls.

Female *Agrp*$^{cre/+}$;*Npy*$^{lox/lox}$ mice in general showed the same metabolic phenotype as male mice but with a somewhat lesser effect size

(Supplementary Figs. 3A–S). Taken together, these data demonstrate that mice lacking *Npy* only in AGRP neurons are still capable of mounting a re-feeding response induced by a negative energy balance. However, even with higher food intake, they are unable to regain the same amount of weight compared with their controls, suggesting that NPY in AGRP neurons is also critical for energy storage and partitioning.

3.2. Lack of *Npy* in AGRP neurons also increases food intake under a positive energy balance

The global *Npy* knockout renders mice resistant to high-fat-diet-induced obesity [19], indicating the strong obesity promoting effects of the NPY system. Therefore, we next investigated how mice that lack *Npy* only in AGRP neurons respond to a positive energy balance by feeding male $Agrp^{cre/+};Npy^{lox/lox}$ and control mice an HFD from 6 weeks of age for a period of 9 weeks. Both $Agrp^{cre/+};Npy^{lox/lox}$ and control mice responded to the higher calorie intake with an increase in body weight gain, and although the $Agrp^{cre/+};Npy^{lox/lox}$ mice were heavier than controls (similarly to that seen in chow-fed mice), the rate of body weight increase was not different between the two genotypes (Figure 2A). All other body composition parameters including total fat and lean mass as well as specific fat depot weights were also not significantly different between genotypes (Figure 2B–E).

Importantly, however, not only was food intake significantly increased in HFD-fed $Agrp^{cre/+};Npy^{lox/lox}$ mice (Figure 2F–G), there was also a shift towards feeding more during the daytime (Figure 2G). In addition, the number of meals eaten during both the light and dark phases was also increased, whereas the size of individual meals was unaltered (Figure 2H–I). Interestingly, although HFD feeding significantly reduced locomotion in control mice compared with their chow-fed counterparts (Figure 2J–K), HFD-fed $Agrp^{cre/+};Npy^{lox/lox}$ mice were not significantly different in this parameter to either their chow-fed counterparts or the HFD-fed control mice (Figure 2J–K). Similarly, HFD feeding eliminated the difference in energy expenditure between $Agrp^{cre/+};Npy^{lox/lox}$ and control mice seen on the chow diet (Figure 2L). This was due to a significant increase in energy expenditure in HFD-fed $Agrp^{cre/+};Npy^{lox/lox}$ mice compared with their chow-fed counterparts (Figure 2M). Although both $Agrp^{cre/+};Npy^{lox/lox}$ and control mice showed the expected reduction in RQ because of HFD consumption during the dark phase (Figure 2N–O), $Agrp^{cre/+};Npy^{lox/lox}$ mice still exhibited a significantly higher RQ during the light phase than HFD-fed controls (Figure 2N–O), which is consistent with their increased daytime feeding.

3.3. Altered bone homeostasis because of the lack of AGRP neuron-derived NPY

Hypothalamic-specific Npy2r-mediated NPY signalling has been shown to be critical for the central control of bone formation [6,20]. However, in contrast to the strong increase in bone mass observed in globally *Npy*-deficient mice, $Agrp^{cre/+};Npy^{lox/lox}$ mice are not significantly different to control mice in either whole body or femur-specific bone parameters under normal chow conditions [21]. In this article, we investigated whether NPY derived from AGRP neurons contributes to the hypothalamic regulation of bone mass under conditions of a positive energy balance, which leads to increased loading on bone because of the elevated body weight. Interestingly, when mice were fed an HFD, the DXA analysis revealed a trend towards an increased femoral bone mineral content (BMC) in $Agrp^{cre/+};Npy^{lox/lox}$ mice compared with the same mice on chow and control mice on an HFD with no change in femur length or femoral BMD (Supplementary Figs. 4A–C). The μCT analysis further showed that $Agrp^{cre/+};Npy^{lox/lox}$ mice were able to increase their cortical bone volume by increasing the cortical thickness in response to the increased body weight associated with the HFD, a change that was not evident in control mice (Supplementary Figs. 4D–E). The trabecular bone volume (BV/TV) was also significantly higher in HFD-fed $Agrp^{cre/+};Npy^{lox/lox}$ mice compared with HFD-fed controls because of protection against a diet-induced reduction in the trabecular number observed in control mice (Supplementary Figs. 4F–H). These data suggest that although AGRP neuron-derived NPY is less critical for bone homeostasis control under basal chow-fed conditions, it is required during a positive energy balance where its reduced levels ensure bone mass increases to match the increase in overall body weight.

3.4. Lack of *Npy* in AGRP neurons delays the onset and amount of feeding

Next, we investigated whether *Npy*-depleted AGRP neurons functionally differ in the way they control feeding and energy homeostasis. For this, we injected $Agrp^{cre/+};Npy^{lox/lox}$ and $Agrp^{cre/+};Npy^{lox/+}$ control mice with a stimulatory AAV-DIO-hM3Dq-mCherry vector (Figure 3A). $Agrp^{cre/+};Npy^{lox/lox}$ mice injected with an empty vector were used as an additional control. The correct injection of the vector was confirmed by the immunohistochemistry evaluation of mCherry (Figure 3B) and functional activation upon Clozapine-N-oxide (CNO) administration by cfos co-staining (Figure 3C–D).

After a 2-week recovery period, 10-week-old male $Agrp^{cre/+};Npy^{lox/lox}$ and $Agrp^{cre/+};Npy^{lox/+}$ mice bilaterally injected with the stimulatory AAV-hM3Dq vector were then tested in the Promethion metabolic phenotyping system. After acclimatisation, half the mice were given interperitonial (ip) CNO and the other half saline, after which food intake, energy expenditure, RQ, and locomotor activity were recorded. Two days later, the experiment was repeated, but in the reversed injection order, so that each mouse acts as its own control. As would be expected, the CNO stimulation of DREADD-injected ($Agrp^{cre/+};Npy^{lox/+}$) control mice led to a quick and significant increase in food intake under both fed and fasted conditions (Figure 3E,Q). Importantly, the increase observed was similar in magnitude (approximately 200%) under both fed and fasted conditions.

Interestingly, when the same experiments were performed on $Agrp^{cre/+};Npy^{lox/lox}$ mice, there was a significant delay in the feeding response. Food intake under fed conditions only increased 3 h after CNO stimulation, and a lower total amount of food was consumed (Figure 3I) compared with CNO-treated $Agrp^{cre/+};Npy^{lox/+}$ control mice (Figure 3E). This suggests that NPY in these neurons specifically contributes to the initiation of feeding but also indicates it is required for continuous feeding. CNO stimulation failed to induce any enhancement in food intake after a fast in the $Agrp^{cre/+};Npy^{lox/lox}$ mice (Figure 3U). This indicates that NPY is required to drive food intake higher under this condition, and that this cannot be compensated for by any of the other factors in these neurons such as AGRP or GABA. Control mice showed a significant increase in energy expenditure under both fed and fasted conditions (Figure 3F,R). Although the CNO stimulation of AGRP neurons in the absence of *Npy* showed a small reduction in EE in the first 2 h after CNO activation in the fed state (Figure 3J), this was unaltered in the fasted state (Figure 3V). Consistent with the strong increase in food intake in the $Agrp^{cre/+};Npy^{lox/lox}$ mice, RQ was also significantly upregulated under both fed and fasted conditions (Figure 3G,S). In addition, and again consistent with their delayed feeding response, the stimulation of AGRP neurons that lack *Npy* also showed a delayed increase in RQ after CNO stimulation in the fed state (Figure 3K), although under fasting conditions, this was not significantly different to when treated with saline (Figure 3W). There was no change in locomotor activity upon CNO activation in the $Agrp^{cre/+};Npy^{lox/lox}$ control mice, either in the

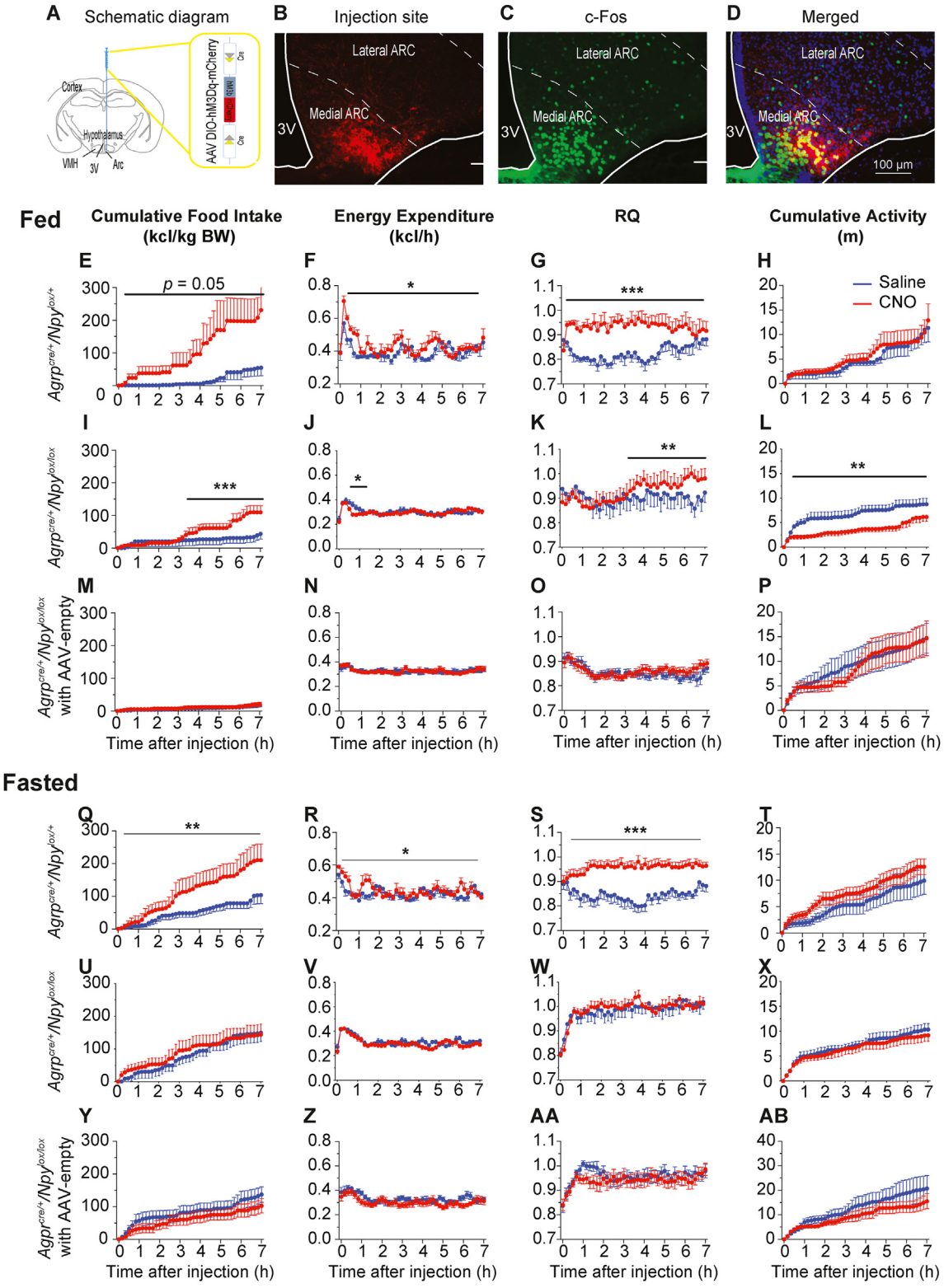

Figure 3: Metabolic profiling of mice selectively lacking *Npy* in AGRP neurons upon DREADD activation. (A) Schematic diagram showing the injection of an AAV-Flex-hM3Dq-mCherry vector into the ARC of *Agrp*$^{cre/+}$;*NPY*$^{lox/lox}$ mice. (B) Fluorescent images showing a successful expression of the DREADD via its co-expressed mCherry protein. (C) The successful activation of DREADD via the CNO ip injection shown by cfos staining (green). (D) A merged image confirming the co-localisation of mCherry and cfos-positive neurons. (E–H) and (Q–T) Food intake, energy expenditure, RQ, and locomotor activity of *Agrp*$^{cre/+}$;*NPY*$^{lox/+}$ mice injected with an AAV-Flex-hM3Dq-mCherry vector and treated with CNO or saline under fed or fasted conditions, respectively. (I–L) and (U–X) Food intake, energy expenditure, RQ, and locomotor activity of *Agrp*$^{cre/+}$;*NPY*$^{lox/lox}$ mice injected with an AAV-Flex-hM3Dq-mCherry vector and treated with CNO or saline under fed or fasted conditions, respectively. (M–P) and (Y-AB) Food intake, energy expenditure, RQ, and locomotor activity of *Agrp*$^{cre/+}$;*NPY*$^{lox/+}$ mice injected with an AAV-empty control vector and treated with CNO or saline under fed or fasted conditions, respectively. Data are means ± SEM of at least 9 per group. * = $p < 0.05$, ** = $p < 0.01$, *** = $p < 0.001$ as indicated.

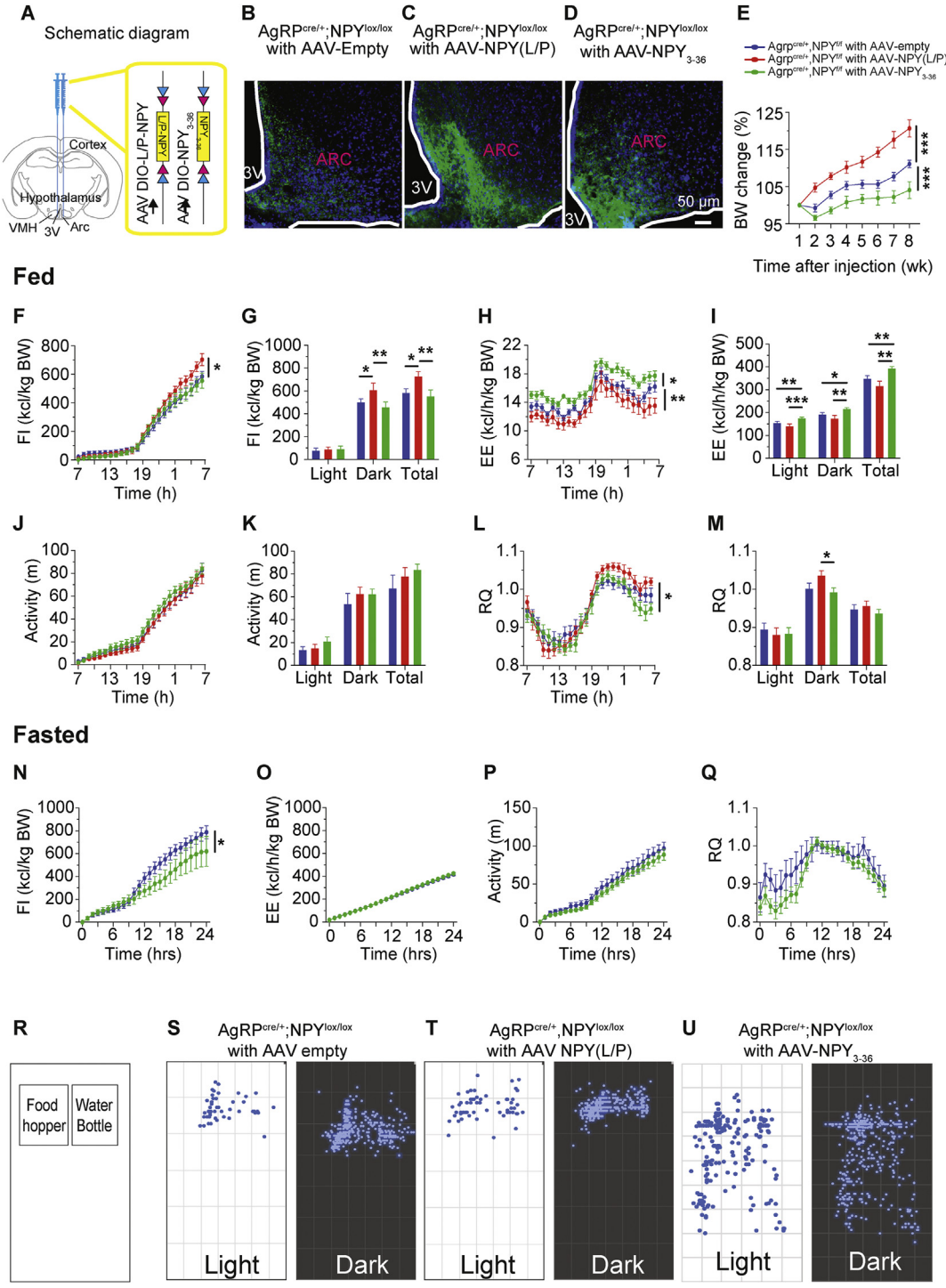

Figure 4: NPY in AGRP neurons controls food intake via Npy1r and energy expenditure via Npy2r pathways. (A) Schematic diagram showing the bilateral delivery of a (Leu [31], Pro [34])NPY, NPY(3—36), or empty FLEX vector into the ARC of *Agrp*$^{cre/+}$;*NPY*$^{lox/lox}$ mice. (B) Fluorescent image showing the expression of *Npy* from AGRP-negative NPY neurons; (C) successful re-introduction of (Leu [31], Pro [34])NPY (L/P) and (D) NPY(3—36) visualized by fluorescent immunohistochemical staining using an anti-NPY AB (green). (E) The body weight gain of *Agrp*$^{cre/+}$;*NPY*$^{lox/lox}$ mice injected with AAV-empty vector (blue), AAV-(Leu [31], Pro [34])NPY (red), and AAV-NPY(3—36) (green). (F) Spontaneous cumulative food intake normalised to the body weight of *Agrp*$^{cre/+}$;*NPY*$^{lox/lox}$ mice with the injection of AAV-empty, AAV-(Leu [31], Pro [34])NPY, and AAV-NPY(3—36); (G) during the light, dark, and over 24 h, respectively. (H) Average energy expenditure over 24 h and (I) cumulative energy expenditure during light and dark phases normalised to body weight. (J) Cumulative locomotor activity and (K) during the light and dark phase. (R) RQ over 24 h and (M) during light and dark phases. (N) Cumulative food intake normalised to the body weight of fasted AAV-NPY(3—36)-injected *Agrp*$^{cre/+}$;*NPY*$^{lox/lox}$ mice. (O) Cumulative energy expenditure, (P) locomotor activity, and (Q) RQ of fasted AAV-NPY(3—36)-injected *Agrp*$^{cre/+}$;*NPY*$^{lox/lox}$ mice. (R) The schematic of the mouse cage indicating a position of food and water hoppers. (S—U) Representative images showing the activity pattern of *Agrp*$^{cre/+}$;*NPY*$^{lox/lox}$ mice injected with an AAV-empty, AAV-(Leu [31], Pro [34])NPY or AAV-NPY(3—36) vector, respectively, during the light and dark phase. Data are means ± SEM of at least 9 per group. * = $p < 0.05$, ** = $p < 0.01$, and *** = $p < 0.001$ as indicated.

fed or fasted state (Figure 3H,T). Interestingly, however, the CNO stimulation of AGRP neurons that lack *Npy* resulted in a significant reduction in locomotor activity in the fed but not fasted state (Figure 3L,X). Control virus-injected *Agrp*$^{cre/+}$;*Npy*$^{lox/lox}$ mice treated with CNO did not show any significant differences to their saline controls in any of the investigated parameters under either fed or fasted conditions (Figure 3M—P,Y-AB).

To test whether inhibiting AGRP neurons in the absence of NPY is able to modulate feeding, we injected an additional cohort of *Agrp*$^{cre/+}$;*Npy*$^{lox/lox}$ mice with an inhibitory AAV-hM4Di vector and repeated the metabolic profiling with these mice. Under fed conditions, activating the inhibitory DREADD with CNO did not result in any significant alterations in food intake, EE, RQ, or physical activity (Supplementary Fig. 4I-L). However, under fasting conditions, inhibiting these Npy-depleted AGRP neurons resulted in a significant decrease in food intake compared with the same mice injected with saline, while not influencing any of the other parameters (Supplementary Fig. 4M-P).

Taken together, these results highlight a feeding stimulatory role for NPY/AGRP neurons, and importantly show that NPY originating from these neurons is critical for the initiation of the feeding response as well as to assure the homeostatic required amount is consumed. However, under fasting conditions, other components of these neurons, most likely AGRP, which does get naturally upregulated under these conditions, may also contribute to the feeding response, which can be blocked via inhibitory DREADD activation. NPY in AGRP neurons seems to be also critical for maintaining locomotor activity, which is likely associated with food foraging behaviours. Furthermore, the preferred choice for carbohydrate utilisation as fuel and the resultant preservation of fat stores seems to also be strongly dependent on the presence of NPY in AGRP neurons.

3.5. Re-introduction of different Y-receptor—preferring NPY ligands identifies Npy1r/Npy5r- and Npy2r-specific controlled pathways

To test whether the re-introduction of NPY can rescue the deletion phenotype but also at the same time to determine which specific Y-receptor signalling pathway is responsible, we re-introduced either the Npy1r/Npy5r-preferring ligand (Leu [31]Pro [34])NPY or the Npy2r-preferring NPY variant NPY(3—36) via AAV-FLEX technology into *Npy*-depleted AGRP neurons of *Agrp*$^{cre/+}$;*Npy*$^{lox/lox}$ mice (Figure 4A). The successful re-expression of the two ligands was confirmed by immunohistochemistry on brain slices from these mice showing extensive positively stained neuronal fibre networks in the ARC compared with *Agrp*$^{cre/+}$;*Npy*$^{lox/lox}$ mice injected with an empty control vector (Figure 4B—D).

Consistent with the prediction of Npy1r/Npy5r activation to drive food intake under normal energy balance conditions, the injection of the AAV-FLEX-(Leu [31]Pro [34])NPY vector into *Agrp*$^{cre/+}$;*Npy*$^{lox/lox}$ mice resulted in a significant increase in body weight when monitored over a 8-week period compared with mice injected with an empty vector (Figure 4E). In contrast, re-introduction of the Npy2r-preferring variant, NPY(3—36), into *Agrp*$^{cre/+}$;*Npy*$^{lox/lox}$ mice did actually lead to reduced body weight gain compared with control virus-injected mice (Figure 4E). The increased body weight in the (Leu [31]/Pro [34])NPY-injected mice was mostly due to a significant increase in spontaneous food intake (Figure 4F,G) and also contributed to by a slight reduction in energy expenditure (Figure 4H,I). Spontaneous food intake was not significantly altered in the NPY(3—36)-replenished mice; however, there was a significant increase in energy expenditure compared with the control-injected mice, which most likely contributed to the slower body weight gain in these mice (Figure 4F—I). Consistent with that, there was a trend in elevated locomotor activity in the NPY(3—36)-replenished mice, but this did not reach significance (Figure 4J,K). Interestingly, and again consistent with the leaner phenotype of the NPY(3—36)-replenished mice, RQ was significantly reduced (Figure 4L,M).

Although there is already a significant increase in food intake observed in the (Leu [31]/Pro [34])NPY-replenished mice, we wondered whether fasting could induce also a feeding drive in NPY(3—36)-replenished mice. Surprisingly, however, fasting actually led to a significant reduction in food intake (Figure 4N). All other parameters such as EE, locomotor activity, and RQ were not significantly different under fasting-refeeding conditions (Figure 4O—Q). Interestingly, however, when analysing other locomotor-related behaviours from the Promethion system, a clear difference in a 24-hour activity pattern was observed in the NPY(3—36) vector-injected, compared with control, or (Leu [31]Pro [34]) NPY vector-injected *Agrp*$^{cre/+}$;*Npy*$^{lox/lox}$ mice (Figure 4R—U). Although control and (Leu [31]Pro [34])NPY vector-replenished mice preferred the area around the food and water hoppers (Figure 4S,T), NPY(3—36) vector-replenished mice showed a wide distribution of activity all around the cage, both during the light as well as the dark phase (Figure 4U), reminiscent of a more explorative phenotype and potentially indicative of an increase in foraging behaviour.

Of note, in addition to (Leu [31]Pro [34])NPY, NPY3-36 does also have affinity for the Npy5r, with an approximately 10-fold lower affinity than (Leu [31]Pro [34])NPY for this receptor [22]. However, it cannot be completely excluded that some aspects of the observed phenotypes in this NPY3-36 re-introduction model have been contributed to by co-stimulation of Npy5r. However, because Npy5r have been shown to stimulate feeding behaviour [23], it is less likely that NPY3-36, which shows a reduction in feeding in our re-introduction model, is a major driver for Npy5r signalling.

Therefore, these results are more consistent with Npy2r auto-receptors on *Agrp*-positive NPY neurons being activated by NPY3-36, which through feedback inhibition reduces the activity of these neurons, subsequently leading to reduced food intake. This is further supported by the strong increase in food intake observed when (Leu [31]Pro [34]) NPY is re-introduced into these *Npy*-depleted AGRP neurons instead (Figure 4F) because this ligand is unable to act on either auto-synaptic or postsynaptic Npy2r but can stimulate postsynaptic Npy1r and to a lesser extend the Npy5r to drive feeding.

3.6. Lack of *Npy* in AGRP neurons leads to the readjustment of Y-receptor expression

The rather paradoxically observed mild obese phenotype mostly driven by the increased food intake and reduced EE and activity in the *Agrp*$^{cre/+}$;*Npy*$^{lox/lox}$ mice suggests potential compensatory mechanisms have been activated. To gain more insights into this possibility, we performed radioactive *in situ* hybridisation experiments and evaluated the expression of *Npy, Agrp*, and *Pomc* mRNA in response to either complete germline *Npy* deletion or selective ablation in AGRP neurons only (*Agrp*$^{cre/+}$;*Npy*$^{lox/lox}$) compared with Wildtype (WT) and *Agrp*$^{cre/+}$;*Npy*$^{lox/+}$ controls. As shown in Figure 5A, *Npy* mRNA expression in *Npy*$^{-/-}$ as expected was completely absent, whereas in the *Agrp*$^{cre/+}$;*Npy*$^{lox/lox}$ mice, it was reduced to approximately 85%, consistent with previous reports that upon selective AGRP neuronal deletion, a subpopulation of AGRP-negative NPY neurons remains [13]. Importantly, *Agrp*$^{cre/+}$;*Npy*$^{lox/+}$mice not significantly differ in *Npy* mRNA expression from WT controls (Figure 5A) confirming them as suitable controls. The deletion of *Npy* specifically in AGRP neurons did not alter the mRNA expression levels of *Npy* anywhere else in the brain, such as the hippocampus (Figure 5B), confirming the specificity of the deletion. Importantly, the lack of *Npy* specifically in AGRP neurons has no effect

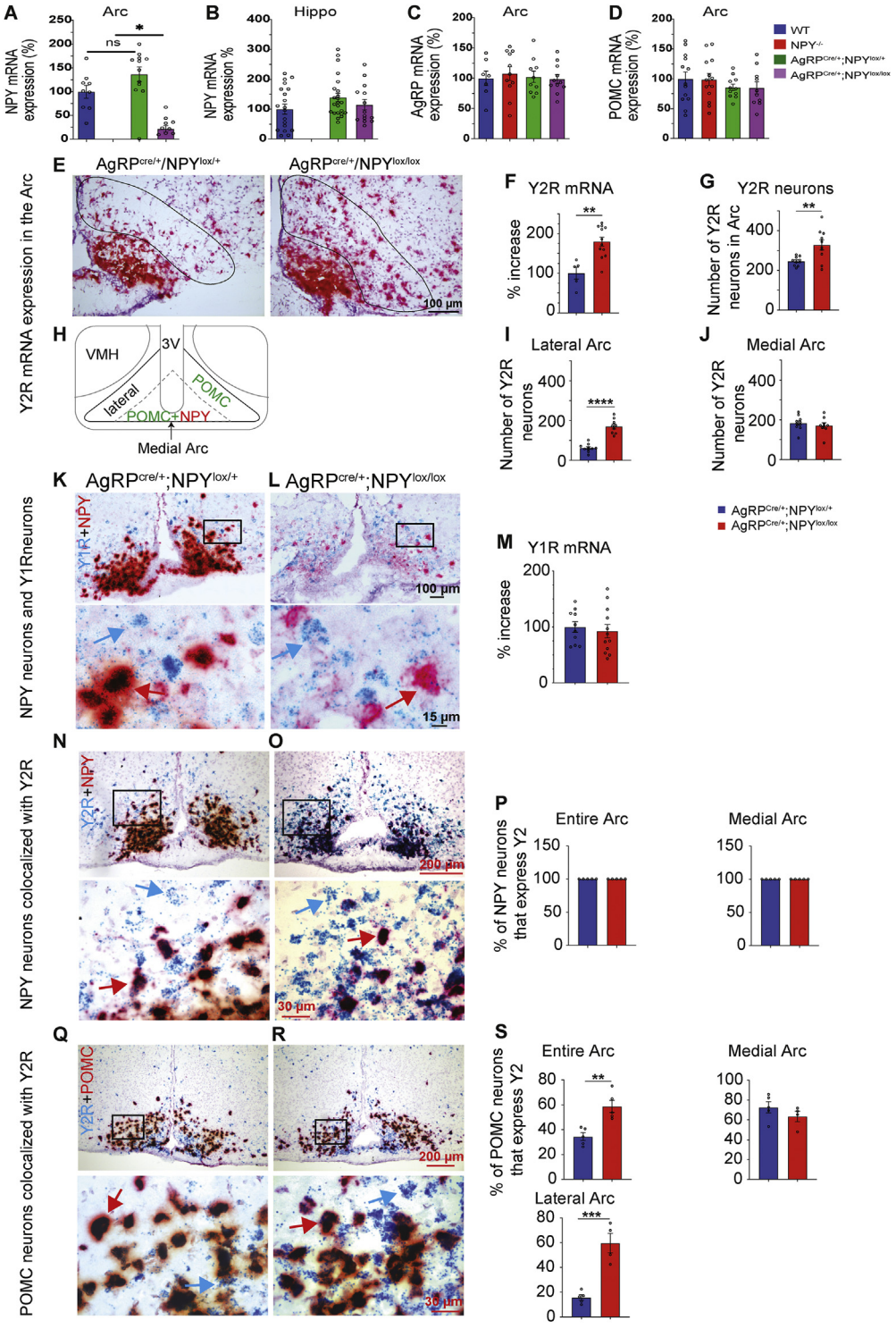

Figure 5: Lack of *Npy* specifically only in AGRP neurons leads to increased *Npy2r* expression. (A,B) The quantification of *Npy* mRNA expression by radioactive *in situ* hybridisation in the ARC and hippocampus of WT, $Npy^{-/-}$, $Agrp^{cre/+}$;$Npy^{lox/+}$ and $Agrp^{cre/+}$;$Npy^{lox/lox}$ mice. (C,D) The quantification of *Agrp* and *Pomc* mRNA expression by radioactive *in situ* hybridisation in the ARC of WT, $Npy^{-/-}$, $Agrp^{cre/+}$;$Npy^{lox/+}$ and $Agrp^{cre/+}$;$Npy^{lox/lox}$ mice. (E) The representative micrograph of the RNAScope™ analysis of Npy2r expression (red) in $Agrp^{cre/+}$;$Npy^{lox/+}$ and $Agrp^{cre/+}$;$Npy^{lox/lox}$ mice using chromogenic detection. (F) The quantification of *Npy2r* and (G) Npy2r neurons in the ARC of $Agrp^{cre/+}$;$Npy^{lox/+}$ and $Agrp^{cre/+}$;$Npy^{lox/lox}$ mice. (H) Schematic defining the areas in the ARC on the coronal neuroanatomic section relative to *Npy* and *Pomc* distribution. (I,J) The quantification of Npy2r neurons in the lateral and medial ARC of $Agrp^{cre/+}$;$Npy^{lox/+}$ and $Agrp^{cre/+}$;$Npy^{lox/lox}$ mice. (K,L) The RNAScope™ co-localisation of *Npy1r* and *Npy* in $Agrp^{cre/+}$;$Npy^{lox/+}$ and $Agrp^{cre/+}$;$Npy^{lox/lox}$ mice using chromogenic detection in low magnification (top) and high magnification of insert (bottom). Blue arrow: *Npy1r* only neuron; red arrow: *Npy/Npy1r* co-localised neuron. (M) The quantification of NPY neurons that co-express Npy1r. (N,O) The RNAScope™ co-localisation of *Npy2r* (blue) and *Npy* (red) in $Agrp^{cre/+}$;$NPY^{lox/+}$ and $Agrp^{cre/+}$;$NPY^{lox/lox}$ mice using chromogenic detection in low magnification (top) and high magnification of the insert (bottom). Blue arrow: *Npy2r* only neuron; red arrow: *Npy/Npy2r* co-localised neuron. (P) The quantification of NPY neurons that co-express *Npy2r*. (Q,R) The RNAScope™ co-localisation of *Npy2r* (blue) and *Pomc* (red) in $Agrp^{cre/+}$;$Npy^{lox/+}$ and $Agrp^{cre/+}$;$Npy^{lox/lox}$ mice using chromogenic detection in low magnification (top) and high magnification of insert (bottom). Blue arrow: *Npy2r* only neuron; red arrow: *Pomc/Npy2r* co-localised neuron. (S) The quantification of *Pomc* neurons that co-express *Npy2r* in the ARC. Data are means ± SEM of at least 5 per group. * = $p < 0.05$, ** = $p < 0.01$, and *** = $p < 0.001$ as indicated.

on the expression of either *Agrp* or *Pomc* under fed conditions (Figure 5C—D), suggesting that NPY produced in AGRP neurons is not required for the control of either *Agrp* or *Pomc* mRNA expression under baseline conditions. This also suggest that *Agrp* and *Pomc* under baseline conditions are unlikely to be responsible for the compensatory effects that led to the increased feeding and mild obesity seen in $Agrp^{cre/+};Npy^{lox/lox}$ mice. However, Agrp mRNA levels are significantly increased upon fasting (data not shown), indicating that the normal responses to a negative energy balance, eg, elevated Ghrelin, is still intact. This is also consistent with unaltered levels of ghrelin receptor mRNA in AGRP neurons of $Agrp^{cre/+};Npy^{lox/lox}$ compared with WT mice (data not shown). We also looked into potential changes in GABA activity and did not observe any major changes in the expression of Gad2 by Quantitative polymerase chain reaction (qPCR) in the $Agrp^{cre/+};Npy^{lox/+}$ mice fed a chow, HFD, or under fasting conditions (Supplementary Fig. 4Q), making GABA signalling a less likely candidate as a major contributor to the observed phenotype.

To further investigate the paradox of an increased feeding drive in the absence of *Npy* in AGRP neurons, we focused on Y-receptor alterations because the global deletion of *Npy* has been shown to lead to significant changes in Y-receptor expression [24]. We used *in situ* hybridisation to examine the expression pattern and level of the 2 most prominent receptors, *Npy1r* and *Npy2r*, in the hypothalamus. Quantifying RNAscope™ data, we identified that *Npy2r* mRNA expression levels (Figure 5E—F) as well as the number of neurons that express *Npy2r* (Figure 5G) in the whole ARC of $Agrp^{cre/+};Npy^{lox/lox}$ mice were significantly increased compared with controls. A further detailed investigation of the distribution of *Npy2r* mRNA expression in $Agrp^{cre/+};Npy^{lox/lox}$ mice revealed a higher density in the lateral part of the ARC where POMC neurons are mostly found (Figure 5H—I), compared with the medial part which has a higher density of NPY neurons (Figure 5J). Importantly, no such changes were observed for the *Npy1r* mRNA with unaltered expression observed between $Agrp^{cre/+};Npy^{lox/lox}$ mice and controls (Figure 5K-M). Similarly, no major change in the expression of the similarly acting Npy5r was observed by qPCR in the $Agrp^{cre/+};Npy^{lox/lox}$ mice (Supplementary Fig. 4R).

To determine whether this strong increase in NPY2R receptor expression was localised to specific neuronal populations, we performed RNAscope™ experiments co-localising *Npy2r* mRNA with either *Npy* or *Pomc* mRNA. Results from these experiments show that *Npy2r* mRNA expression can be found on both AGRP-positive as well as AGRP-negative NPY neurons, irrespective of their medial-lateral aspect on location (Figure 5N—P). In contrast, POMC neurons that are predominantly expressed in the lateral part of the ARC show only a partial co-localisation with *Npy2r* mRNA in control mice, i.e., ~36% (Figure 5Q—S). Interestingly, the level of co-expression of *Pomc* and *Npy2r* mRNA showed a 1.7-fold increase in $Agrp^{cre/+,}Npy^{lox/lox}$ mice, with ~61% POMC neurons co-expressing *Npy2r* mRNA in the lateral ARC (Figure 5Q—S). Together, these data demonstrate that the lack of the available NPY ligand derived from AGRP neurons triggers an increase in *Npy2r* expression in the ARC, more so in POMC neurons.

3.7. ARC *Npy2r* expression is upregulated under both positive and negative energy balances

To also investigate whether *Npy2r* expression is influenced by energy status, we fed $Agrp^{cre/+};NPY^{lox/lox}$ and $Agrp^{cre/+};NPY^{lox/+}$ control mice an HFD for 3 weeks and performed RNAScope for *Npy2r* expression co-localised with *Npy* as well as *Pomc*-positive neurons. As shown in Supplementary Fig. 5, *NPY* mRNA levels were reduced as expected in response to a short-term HFD in both genotypes; however, a strong overlap in *Npy2r* and *Npy* expression under these conditions can still observed. Importantly, the already elevated *Npy2r* expression in the $Agrp^{cre/+};NPY^{lox/lox}$ mice was further enhanced by the obesifying effect of the HFD (Supplementary Figs. 5C and D). *Pomc* mRNA expression on the other hand is slightly diminished in response to an HFD, in both $Agrp^{cre/+};NPY^{lox/+}$ and $Agrp^{cre/+};NPY^{lox/lox}$ mice (Supplementary Figs. 6A—D). However, the co-localisation of *Pomc* with *Npy2r* was further enhanced under these conditions, especially in the $Agrp^{cre/+};NPY^{lox/lox}$ mice (Supplementary Fig. 6D).

We next investigated *Npy2r* levels under fasting conditions. Interestingly, fasting also increased *Npy2r* in both $Agrp^{cre/+};NPY^{lox/lox}$ and $Agrp^{cre/+};NPY^{lox/+}$ control mice to a similar extend but again with higher absolute levels in the $Agrp^{cre/+};NPY^{lox/lox}$ mice (Supplementary Figs. 7A and B). As expected, fasting also increased the levels of *NPY* mRNA in both genotypes, with a greater extent in the $Agrp^{cre/+};NPY^{lox/lox}$ mice (Supplementary Figs. 7A and B). Importantly, Npy2r did highly co-localise with these *Agrp*-negative *NPY* neurons and also appear to be predominantly GABA-ergic (Supplementary Fig. 7A), although very little glutamatergic co-localisation could be observed (Supplementary Fig. 7B). Fasting reduced *Pomc* mRNA expression (Supplementary Fig. 8), but again *Npy2r* could be found upregulated and highly co-localised with these *Pomc* neurons (Supplementary Fig. 8), and, similarly to the *Agrp*-negative NPY neurons, these *Pomc* neurons are predominantly GABA-ergic (Supplementary Fig. 8). Taken together, these results show that *Npy2r* expression is highly regulated by energy status and surprisingly is upregulated under both positive as well as negative energy balance conditions.

4. DISCUSSION

This is the first study that describes the specific function of NPY derived from AGRP neurons based on the selective ablation of the *Npy* gene only in this group of neurons. Contrary to what would be expected from the lack of an orexigenic acting neurotransmitter, mice lacking *Npy* only in AGRP neurons actually develop a mild obese phenotype contributed to by increased food intake and reduced energy expenditure and activity. Importantly, under a positive energy balance, food intake was still significantly elevated, mostly because of the increased bout number and interestingly also a shift to increased daytime feeding, suggesting that NPY in AGRP neurons may also contribute to the circadian aspects of feeding behaviour [25].

Fasting-induced food intake, although delayed in onset, was otherwise not affected in $Agrp^{cre/+};Npy^{lox/lox}$ mice, and actually even resulted in higher food intake over a 24-hour re-feeding period, suggesting potential compensatory mechanisms were activated. On the other hand, body weight re-gain after fasting was impaired, indicating that NPY in these neurons is critical for energy storage and partitioning. Our results also show that NPY released from AGRP neurons is critical for initiating feeding under baseline fed conditions because chemogenetically, activating *Npy*-deficient AGRP neurons in mice showed a significantly delayed onset and lower amplitude of food intake compared with controls. The delayed onset in feeding in the absence of NPY is not likely to be driven by GABA action because this would be expected to be immediate [26]. On the other hand, the co-localised Agrp that has been shown to act as an inverse agonist on MC3R and MC4R [27,28] has a slower mode of action and thus is likely the major driver for food intake in the absence of NPY from these neurons. Consistent with a role for NPY in AGRP neurons in regulating energy expenditure and locomotor activity, both of which were observed to be reduced in the $Agrp^{cre/+};Npy^{lox/lox}$ mice under baseline conditions, DREADD activation failed to increase these parameters.

One striking alteration observed because of the lack of *Npy* in AGRP neurons was a strong upregulation of *Npy2r* mRNA in the ARC. This is consistent with findings in global germline *Npy* knockout mice where Npy2r density increased in the hypothalamus of these mice [24]. Npy2r is known to be expressed on AGRP/NPY neurons where they have been proposed to mediate the satiety-inducing action of peripherally derived PYY and PYY(3—36) [29]. In addition, Npy2r on NPY neurons are believed to also act as auto-receptors in a feedback loop to control expression of *Npy2r* and release of NPY from these neurons [30]. Importantly, the activation of these Npy2r auto-receptors by NPY(3—36) re-introduction led to an enhanced inhibitory action of these NPY neurons, thereby reducing their ability to promote food intake. This is also consistent with the opposing effect seen when re-introducing the Npy1r/Npy5r receptor-preferring ligand (Leu [31]Pro [34])NPY into the ARC of $Agrp^{cre/+};Npy^{lox/lox}$ mice, which does not have the ability to act on Npy2r auto-receptors, thereby being unable to inhibit these neurons, but importantly, still being able to drive food intake via actions on postsynaptic Npy1r/Npy5r. Furthermore, the conditional deletion of *Npy2r* specifically in NPY neurons of adult animals has been shown to affect fasting-induced, but not spontaneous feeding [31], in line with the observed reduced response to this intervention in our DREADD study on $Agrp^{cre/+};Npy^{lox/lox}$ mice.

More importantly, *Npy2r* expression was specifically increased in POMC neurons, which is likely the major contributing factor to the observed mild obese phenotype of the $Agrp^{cre/+};Npy^{lox/lox}$ mice, because it has been shown that the activation of Npy2r on POMC neurons has a stimulatory effect on feeding [32]. Consistent with this, the chronic intracerebroventricular (ICV) infusion of the Npy2r-preferring ligand PYY(3—36) has been shown to lead to an increase in food intake and the development of obesity [33]. It remains to be determined which NPY source is responsible for the activation of Npy2r on POMC neurons in the $Agrp^{cre/+};Npy^{lox/lox}$ mice, but the remaining AGRP-negative NPY neurons represent a plausible candidate.

Previous studies have shown that AGRP/NPY neurons actually become silent as soon as food becomes available [34], and a recent study using optogenetic tools also suggests that NPY derived from AGRP neurons is essential for a sustained feeding drive because the re-introduction of NPY into these neurons rescued the feeding phenotype, whereas the chemogenetic activation of feeding is not affected by the lack of *Npy* [4]. This is in contrast to our results using chemogenetics. Some of the discrepancies can probably be explained by the use of different mouse models. In the model used by Chen et al.; global germline *Npy* knockout mice were crossed with an *Agrp*-Cre line, resulting in a lack of *Npy* everywhere and not only in the AGRP neurons, whereas our model selectively removed *Npy* only in AGRP neurons, leaving it unaltered everywhere else. As such, the re-introduction of *Npy* into AGRP neurons on the background of a global lack of *Npy* does not account for any contributions from any other *Npy* sources. Furthermore, the global *Npy* knockout results in the strong deregulation of *Npy1r* and *Npy2r* expression, which may result in different responses to when *Npy* is selectively only re-introduced in AGRP neurons to what is observed under normal Y-receptor expression levels. Finally, optogenetic and chemogenetic stimulation leads to potentially different modes of action, and this, combined with the different genetic models and the timeline over which food intake was investigated in the optogenetic versus the chemogenetic activation, may add up to produce the observed different outcomes.

Another study also utilising a global germline *Npy* knockout crossed with an *Agrp*-Cre line [14] and combined that with a germline cross to a chemogenetic DREADD transgene did partially confirm our results of NPY derived from AGRP neurons being required for feeding as well as its critical involvement in regulating glucose homeostasis. However, in that model, the strong dependence of AGRP neuron-derived NPY for maintaining locomotor activity we identified was not observed. Again, the rather different nature of the two models, germline introduction of DREADD versus viral delivery in the adult, on top of the global lack of *Npy* in their model, may have been the main reasons for the discrepancies. Taken together, our study has shown that NPY derived from AGRP neurons is critical for food seeking, initiating feeding and altering energy expenditure to protect energy stores in the form of fat as well as maintaining basic activity levels. Furthermore, NPY originating from AGRP neurons is involved in the control of glucose homeostasis and is necessary to match bone mass to increased body weight. The observed changes in corresponding Y-receptor expression because of alteration in NPY ligand availability is also an important finding from this study, highlighting the separation of functions by using different Y-receptor controlled pathways. In addition, the alteration of Y-receptor expression in this model also demonstrates that the regulation of energy homeostasis involves a variety of responses and adaptations to adjust energy balance in response to varying energy supply, which goes beyond the simple elevation or reduction in neurotransmitter availability.

AUTHOR CONTRIBUTION

Conceptualization, H.H and L.Z.; methodology, H.H., Y.Q., L.Z., and C.I.; investigation, Y.Q., C.I., R.E., N.L., and L.Z.; writing, H.H., L.Z., Y.Q., and N.L.; funding acquisition, H.H. and L.Z.; resources, R.T.; and supervision, H.H., L.Z., Y.Q., N.L., and C.I.

FUNDING

This research was supported by the National Health and Medical Research Council (NHMRC) with project grant #1144819 and a research fellowship to H.H. #1118775.

ACKNOWLEDGMENTS

We thank the staff of the Garvan Institute Biological Testing Facility and staff of the Australian BioResources for taking care of our test mice. We thank Ms Jennifer Lee for technical assistance.

CONFLICT OF INTEREST

None declared.

APPENDIX A. SUPPLEMENTARY DATA

Supplementary data to this article can be found online at https://doi.org/10.1016/j.molmet.2022.101455.

REFERENCES

[1] Spiegelman, B.M., Flier, J.S., 2001. Obesity and the regulation of energy balance. Cell 104:531—543.

[2] Herzog, H., 2020. Integrated pathways that control stress and energy homeostasis. Nature Reviews Endocrinology 16:75—76.

[3] Loh, K., Herzog, H., Shi, Y.C., 2015. Regulation of energy homeostasis by the NPY system. Trends in Endocrinology and Metabolism 26:125—135.

[4] Chen, Y., Essner, R.A., Kosar, S., Miller, O.H., Lin, Y.C., Mesgarzadeh, S., et al., 2019. Sustained NPY signaling enables AgRP neurons to drive feeding. Elife 8.

[5] Lee, N.J., Herzog, H., 2020. Coordinated regulation of energy and glucose homeostasis by insulin and the NPY system. Journal of Neuroendocrinology 33:e12925.
[6] Lee, N.J., Herzog, H., 2009. NPY regulation of bone remodelling. Neuropeptides 43:457–463.
[7] Dietrich, M.O., Zimmer, M.R., Bober, J., Horvath, T.L., 2015. Hypothalamic Agrp neurons drive stereotypic behaviors beyond feeding. Cell 160:1222–1232.
[8] Horio, N., Liberles, S.D., 2021. Hunger enhances food-odour attraction through a neuropeptide Y spotlight. Nature 592:262–266.
[9] Zhang, L., Hernandez-Sanchez, D., Herzog, H., 2019. Regulation of feeding-related behaviors by arcuate neuropeptide Y neurons. Endocrinology 160:1411–1420.
[10] Erickson, J.C., Clegg, K.E., Palmiter, R.D., 1996. Sensitivity to leptin and susceptibility to seizures of mice lacking neuropeptide Y. Nature 381:415–421.
[11] Qian, S., Chen, H., Weingarth, D., Trumbauer, M.E., Novi, D.E., Guan, X., et al., 2002. Neither agouti-related protein nor neuropeptide Y is critically required for the regulation of energy homeostasis in mice. Molecular and Cellular Biology 22:5027–5035.
[12] Bewick, G.A., Gardiner, J.V., Dhillo, W.S., Kent, A.S., White, N.E., Webster, Z., et al., 2005. Post-embryonic ablation of AgRP neurons in mice leads to a lean, hypophagic phenotype. The FASEB Journal 19:1680–1682.
[13] Luquet, S., Perez, F.A., Hnasko, T.S., Palmiter, R.D., 2005. NPY/AgRP neurons are essential for feeding in adult mice but can be ablated in neonates. Science 310:683–685.
[14] Engstrom Ruud, L., Pereira, M.M.A., de Solis, A.J., Fenselau, H., Bruning, J.C., 2020. NPY mediates the rapid feeding and glucose metabolism regulatory functions of AgRP neurons. Nature Communications 11:442.
[15] Ip, C.K., Zhang, L., Farzi, A., Qi, Y., Clarke, I., Reed, F., et al., 2019. Amygdala NPY circuits promote the development of accelerated obesity under chronic stress conditions. Cell Metabolism 30:111–128 e116.
[16] Tong, Q., Ye, C.P., Jones, J.E., Elmquist, J.K., Lowell, B.B., 2008. Synaptic release of GABA by AgRP neurons is required for normal regulation of energy balance. Nature Neuroscience 11:998–1000.
[17] Paxinos, G., Franklin, K.B.J., Franklin, K.B.J., 2001. The mouse brain in stereotaxic coordinates, 2nd. San Diego: Academic Press.
[18] Lee, N.J., Nguyen, A.D., Enriquez, R.F., Luzuriaga, J., Bensellam, M., Laybutt, R., et al., 2015. NPY signalling in early osteoblasts controls glucose homeostasis. Molecular Metabolism 4:164–174.
[19] Zhang, L., Lee, I.C., Enriquez, R.F., Lau, J., Vähätalo, L.H., Baldock, P.A., et al., 2014. Stress- and diet-induced fat gain is controlled by NPY in catecholaminergic neurons. Molecular Metabolism 3:581–591.
[20] Baldock, P.A., Sainsbury, A., Couzens, M., Enriquez, R.F., Thomas, G.P., Gardiner, E.M., et al., 2002. Hypothalamic Y2 receptors regulate bone formation. Journal of Clinical Investigation 109:915–921.
[21] Enriquez, R.F., Lee, N.J., Herzog, H., 2021. AgRP signalling negatively regulates bone mass. Journal of Neuroendocrinology 33:e12978.
[22] Hu, Y., Bloomquist, B.T., Cornfield, L.J., DeCarr, L.B., Flores-Riveros, J.R., Friedman, L., et al., 1996. Identification of a novel hypothalamic neuropeptide Y receptor associated with feeding behavior. Journal of Biological Chemistry 271:26315–26319.
[23] Nguyen, A.D., Mitchell, N.F., Lin, S., Macia, L., Yulyaningsih, E., Baldock, P.A., et al., 2012. Y1 and Y5 receptors are both required for the regulation of food intake and energy homeostasis in mice. PLoS One 7:e40191.
[24] Trivedi, P.G., Yu, H., Trumbauer, M., Chen, H., Van der Ploeg, L.H., Guan, X., et al., 2001. Differential regulation of neuropeptide Y receptors in the brains of NPY knock-out mice. Peptides 22:395–403.
[25] Edelsbrunner, M.E., Painsipp, E., Herzog, H., Holzer, P., 2009. Evidence from knockout mice for distinct implications of neuropeptide-Y Y2 and Y4 receptors in the circadian control of locomotion, exploration, water and food intake. Neuropeptides 43:491–497.
[26] Krashes, M.J., Shah, B.P., Koda, S., Lowell, B.B., 2013. Rapid versus delayed stimulation of feeding by the endogenously released AgRP neuron mediators GABA, NPY, and AgRP. Cell Metabolism 18:588–595.
[27] Breit, A., Wolff, K., Kalwa, H., Jarry, H., Büch, T., Gudermann, T., et al., 2006. The natural inverse agonist agouti-related protein induces arrestin-mediated endocytosis of melanocortin-3 and -4 receptors. Journal of Biological Chemistry 281:37447–37456.
[28] Smith, M.A., Hisadome, K., Al-Qassab, H., Heffron, H., Withers, D.J., Ashford, M.L., et al., 2007. Melanocortins and agouti-related protein modulate the excitability of two arcuate nucleus neuron populations by alteration of resting potassium conductances. Journal of Physiology 578:425–438.
[29] Batterham, R.L., Cowley, M.A., Small, C.J., Herzog, H., Cohen, M.A., Dakin, C.L., et al., 2002. Gut hormone PYY(3-36) physiologically inhibits food intake. Nature 418:650–654.
[30] King, P.J., Widdowson, P.S., Doods, H.N., Williams, G., 1999. Regulation of neuropeptide Y release by neuropeptide Y receptor ligands and calcium channel antagonists in hypothalamic slices. Journal of Neurochemistry 73:641–646.
[31] Qi, Y., Fu, M., Herzog, H., 2016. Y2 receptor signalling in NPY neurons controls bone formation and fasting induced feeding but not spontaneous feeding. Neuropeptides 55:91–97.
[32] Ghamari-Langroudi, M., Colmers, W.F., Cone, R.D., 2005. PYY3-36 inhibits the action potential firing activity of POMC neurons of arcuate nucleus through postsynaptic Y2 receptors. Cell Metabolism 2:191–199.
[33] Raposinho, P.D., Pierroz, D.D., Broqua, P., White, R.B., Pedrazzini, T., Aubert, M.L., et al., 2001. Chronic administration of neuropeptide Y into the lateral ventricle of C57BL/6J male mice produces an obesity syndrome including hyperphagia, hyperleptinemia, insulin resistance, and hypogonadism. Molecular and Cellular Endocrinology 185:195–204.
[34] Chen, Y., Lin, Y.C., Kuo, T.W., Knight, Z.A., 2015. Sensory detection of food rapidly modulates arcuate feeding circuits. Cell 160:829–841.

